Estimating Horizontal Gradients of Tropospheric Path Delay with a Single GPS Receiver

Yoaz E Ikir-Sever', Peter M. Kroger[1] and Jorgen A. Borjesson[2]

[1]Jet Propulsion Laboratory, California Institute of Technology

[2]Onsala Space Observatory, Chalmers Universit y of Technology, Sweden

Submitted to the *Journal of Geophysical Research, 1997*

Contact:
Yoaz E. Bar-Sever
M.S. 238-600
JPL
Pasadena, CA911 09
Tel: (81 8) 354-2665
Fax: (818) 393-4965
email: yeb@cobra.jpl.nasa.gov

November 7, 1997

Abstract

We present evidence that modeling troposphere delay gradients in precise GPS geodesy can improve the accuracy and precision of the estimated quantities. We also present evidence that the gradient estimates resemble real atmospheric moisture gradients observed with a water vapor radiometer. The geodetic results are based on massive point-positioning experiments, processing three months worth of data from about 150 global IGS sites. Wc used comparisons with water vapor radiometers as an independent measure of solution accuracy. Several estimation strategies were tested, some that account for troposphere gradients and some that do not. We found that using a low elevation angle cutoff, combined with a mode] of the atmospheric delay gradient as a random walk process leads to 19.5% and 1570 average improvement in radial and horizontal site position repeatabilities, respectively, relative to a current state-of-the-art estimation strategy that does not model horizontal gradients and imposes high elevation angle cutoff. The agreement between estimated values of zenith wet delay from collocated GPS receivers and Water Vapor Radiometers (WVR) was improved by at least 25% for our two test sites. Wc also found that merely lowering the elevation angle cutoff improves the repeatabilit y of the radial component of the site's position vector, but tends to degrade the repeatability of the horizontal components of the position vector if the troposphere gradient is not properly modeled. The validation of the GPS-based estimates of troposphere delay gradients is based on comparisons between the GPS receiver at Onsala, Sweden, and a collocated WVR, during October, 1995. The GPS solution seems to track well the fluctuations of moisture gradients over time scales as short as 15 minutes. The agreement in azimuth between the GPS-based and the WVR-based gradients was at the 10° level, for significant gradients. The GPS was found to under-estimate the magnitude of the gradients by about 60% relative to the WVR-based gradients. The ability to sense atmospheric moisture gradients from a single GPS receiver increases the useful information content from networks of GPS receivers by providing additional spatial information for weather forecasting applications.

Introduction

The Global Positioning System (GPS) has reached operational status in early 1994, and is now operating continuously with the full 24-satellite constellation. An explosion in the number of applications has transformed the system from a mere navigation tool to a valuable remote sensing system. Traditionally used for high precision geodesy, the GPS system has recently emerged as a powerful tool in atmospheric studies, in particular, climatology and meteorology. In fact, the geodetic and atmospheric. applications of the GPS cannot be separated; to get the precise location of the receiver, the delay suffered by the GPS signal while traversing the atmosphere must be accurately known.

The main meteorological product of groun(i-based GPS is the estimate of Precipitable Water vapor (PW), the vertically integrated quantity of atmospheric water vapor. Using ancillary measurements of surface pressure and temperature, PW is inferred from values of Total Zenith Delay (TZD) which are directly estimated from the GPS data. Its high temporal resolution, proven all-weather high accuracy and low cost, make grouncl-based GPS a uniquely powerful system for the observation of water vapor.

The TZD is the atmospheric delay of a GPS signal arriving from the zenith direction. It can be separated into two components, a delay due to the dry gases in the troposphere and the non-dipole component of water vapor refractivity, denoted as zenith hydrostatic delay (D_{hz}), and a delay due to the dipole component of water wiper refractivity in the atmosphere, denoted as zenith wet delay (D_{wz}) [Davis et al., 1985]. The zenith hydrostatic delay can be accurately inferred from precise measurements of surface atmospheric pressure using the formula:

$$D_{hz} = 0.22765\ P\ /(1 - 0.00266 \cos 2\lambda - 0.00028\ h),$$

where P is surface pressure in mbar, λ is the latitude, h is geodetic height in km, and D_{hz} is given in cm [Saastamoinen, 1972]. After removing the hydrostatic delay from the total delay, the remaining zenith wet delay is nearly proportional to the PW, the quantity of water vapor integrated along the zenith direction, i.e.,

$$PW = \pi * D_{wz},$$

[Bevis et al., 1994]. **The** proportionality factor, π, is a weak function of T_m, the weighted mean temperature of the atmosphere column,

$$\pi = 10^6 / (p\ R_v (k2' + k3 / T_m)),$$

where k2' and k3 arc empirical physical constants, p is the density of liquid water, and R_v is the specific gas constant for water vapor. Bevis ct al. [1994] have derived the following regression formula to approximate T_m from values of surface temperature:

$$T_m = 0.72\ t + 70.2\ (^0K).$$

The connection between the line-of-sight delay for the individual satellite-receiver link, D_L, and the zenith delay parameters, D_{hz} and D_{wz}, is made through the "hydrostatic" and "wet" mapping functions $m_h(e)$ and $m_w(e)$, respectively, i.e.,

$$D_L = m_h(e)*D_{hz} + m_w(e)*D_{wz}, \qquad (1)$$

where e is the elevation angle, measured from the local horizon to the line-of-sight. Several such mapping functions exist, and the most commonly used in precise geodetic applications are those derived by Lanyi [1984], Herring [1992] and Niell [1996]. The zenith hydrostatic delay component, D_{hz}, typically accounts for about 90% of the total delay at any given site and, as mentioned above, is highly predictable based on surface pressure. The zenith wet delay, although relatively small (typically lcss than 30 cm), is highly variable and unpredictable. In precise GPS applications where

millimeter accuracy is desired, the zenith wet delay must be estimated with the other geodetic quantities of interest.

The only variable in equat ion (1) is the elevation angle, revealing the underlying assumption that the at mosphere is azimuthal] y homogeneous. Azimuthal l y inhomogeneous mapping functions have been proposed as early as 1977 [Gardner] but have never been used in routine GPS geodesy, although a successful application of an azimuthally inhomogeneous atmosphere mapping function in VLBI was reported by Chen and Herring [1997] and MacMil Ian [1995]. Several recent studies have pointed to mismodeling of the troposphere delay as one of the largest error sources in precise GPS geodesy [Ware et al., 1997, Bar-Sever, 1996, Heflin et al. 1996, Heflin et al., 1994].

In this paper wc evaluate the errors in geodetic applications caused by the assumption of azimuthal homogeneity in the troposphere mapping functions, and we present an improved model. We do so by adding to the homogeneous mapping function a simple azimuthally-dependent component representing a horizontal gradient in the tropospheric delay. We usc the precise point positioning technique [Zumberge et al., 1997] to demonstrate that under certain conditions, using the gradient model significantly improves important aspects of solution quality. In doing so, we address the controversial issue of low elevation angle tracking, and present yet another piece of evidence in support of lowering elevation angle cutoff values despite the increase in multipath and the reduction in signal-to-noise ratio that accompanies low elevation measurements. We also present preliminary results demonstrating that the observed gradients represent real atmospheric features, and are not artifacts caused by other errors such as multipath and GPS orbital errors. Whereas the traditional estimation of zenith delay supplies one-dimensional vertical information, estimating the horizontal gradient adds information about the horizontal dimension. This increases the useful information content from networks of GPS receivers anti increases the utility of ground-based GPS measurements for weather forecast i ng.

The gradient model is described in the next section, followed by sections describing the set-up and results from a series of experiments designed to test the impact of the gradient model on precise point positioning. We then proceed to evaluate the accuracy of the estimated gradients using data from a Water Vapor Radiometer (WVR). We end with a discussion of the results.

The gradient model

Following MacMillan [1995], the delay in the GPS signal due to the troposphere gradient is modeled as,

$$\Delta D = m_{\Delta}(e) \cot e \, [G_N \cos \phi + G_E \sin \phi]$$

where ϕ is the azimuth angle measured eastward from north. The reason behind the name "gradient model" can easily be seen if wc rewrite the model as

$$\Delta D = \text{lll}A(C) \cot e \, |G| \langle U_G, U_\phi \rangle,$$

where $G = (G_N, G_E)$ is the gradient vector, $U_\phi = (\cos \phi, \sin \phi)$ is the azimuth vector, $U_G = G/|G|$, and $\langle\ \rangle$ indicates an inner (dot) product. The magnitude of ΔD is greatest when the azimuth vector points along the gradient vector, and ΔD is zero when the azimuth vector is perpendicular to the gradient vector.

Together with the homogeneous terms the complete model for the line-of-sight delay is

$$D_L = m_h(e) D_{hz} + m_w(e) D_{wz} + m_{\Delta}(e) \cot e \, [G_N \cos \phi + G_E \sin \phi]. \qquad (2)$$

We implemented this model in JPL's GIPSY OASIS software where we chose m_h and m_w to be Niell's hydrostatic and wet mapping functions, respectively [Niell, 1996]. We chose $m_\Delta = m_w$ although the choice of m_h gave essentially the same results. Chen and Herring [1997] discuss an alternative inhomogeneous mapping function that avoids the singularity at zero elevation angle. They apply it to VLBI data and validate it by comparisons to three-dimensional weather analysis fields. We did not attempt to evaluate their mapping function here.

It is evident from equation (2) that observations from sufficiently low elevation angles are required in order to separate the gradient components from the azimuthally homogeneous components. MacMillan [1995] processed VLBI data down to 5° with this model and obtained the best performance with a 7° elevation angle cutoff. We also chose 7° as the elevation angle cutoff to be used with this model. At 7° elevation, a gradient with a magnitude of 1 mm corresponds to slant path delay of 67 mm.

Estimation strategies and experiment set-up

Many different approaches have been used to estimate the troposphere delay from GPS data. They usually differ in the choices of the temporal model for the delay and the elevation angle cutoff. The variety of temporal models commonly used range from a 2-hour piecewise constant model to a random walk model with updates every 5 minutes. Elevation angle cutoff values are typically 20° or 15°'

We experimented with a number of estimation strategies to evaluate the performance of the gradient model. All can be viewed as variants of the strategy currently employed at JPL for routine, precise

positioning of ground sites (see below). All the experiments are carried out using the technique of point-positioning. This powerful technique allows for rapid determination of a site's position, clock and troposphere delay parameters using previously-determined GPS orbits and clocks [Zumberge et al., 1997]. The dependence of the GPS orbits and clock on the particular troposphere model used in the "global solution" is weak due to the large number (-40) of sites used in the global solution. We have verified that GPS orbits and clock arc insensitive to variations in receiver elevation angle cutoff but they do improve somewhat (see below) when gradients are modeled. For the fixed GPS orbits and clocks we used the JPL precise solutions for the IGS [Zumberge et al., 1995]. These orbits and clocks solutions were produced without the gradient model.

The various estimation strategies wc experimented with arc described below. Each is assigned a name that will be used later in the text to refer to that strategy. Table 1 summarizes the differences between the various estimat ion strategies employed in our experiments.

Current JPL: The current JPL routine processing strategy for precise point positioning of a given site uses 24 hours of data from the ground receiver, centered around noon, UTC. Phase measurements are selected once every five minutes and pseudorange measurements are carrier-smoothed to the five-minute mark. An elevation angle cutoff value of 15° is used and the troposphere mapping function is that of Lanyi [1984]. The site's position vector is estimated daily as a constant. The receiver's clock is modeled as a white noise process with updates at every measurement epoch, and the wet zenith delay, D_{wz}, is modeled as random walk with unconstrained a-priori and a random walk sigma of 10.2 mm/√hour. A post-fit residual window filters out all phase measurements with post-fit error larger than 5 cm [Zumberge et al., 1995]. (In our experiments with the current JPL strategy we replaced Lanyi's mapping function with that of Niell [1996]. The impact of this switch is negligible). (Please see Note in the discussion section regarding recent changes to JPL's estimation strategy.)

Nominal homogeneous: This strategy is identical to the current JPL strategy but with elevation angle cutoff reduced to 7“, and random walk sigma for D_{wz} reduced to 3 mm/√hour. This was found to be consistently superior to the current JPL strategy [Bar-Sever, 1996, Bar-Sever et. al., 1996].

Nominal inhomogeneous: This was our first attempt at estimating the troposphere gradients. This strategy is identical to the nominal homogeneous strategy, but in addition to the wet zenith delay, D_{wz}, we solve for the two components of the gradient vector, G_N and G_E, modeled as random walk processes, with unconstrained a-priori and a random walk sigma of 0.6 mm/√hour.

Constant gradient: This strategy estimates a single daily gradient. It is identical to the nominal inhomogeneous strategy, except that the gradient is modeled as constant over a day. We included this strategy to provide an alternative strategy for those who do not use stochastic models.

Tuned inhomogeneous: This strategy is identical to the nominal inhomogeneous strategy but the random walk sigma for the gradient parameters is reduced to 0.3 mm/√hour and the post-fit residual window is reduced to 2.5 cm. This was made in an effort to improve the performance of the gradient model.

Tuned 15: This strategy is identical to the tuned inhomogeneous strategy except that the elevation angle cutoff was raised to 15°. This strategy was used in order to check if the benefits of the tuned inhomogeneous strategy persist at a higher elevation angle cutoff.

We designed a series of experiments to assess the impact of the troposphere gradient model on the estimate of a site’s position. in the absence of truth values we evaluate the above 6 strategies mainly

through their internal consistency, namely, the day-to-day repeatability of the site positions. In isolated cases wc were able to compare GPS-based estimates of troposphere delay to those derived from a collocated WVR, thus establishing a more direct evaluation of performance through a comparison with an independent technique.

The data set for our experiments comprises measurements from all IGS sites (-150) available during October - December, 1996. This resulted in about 13500 site-days. In the experiments described below we point-positioned a sub-set of all of the IGS sites during this period to form a statistically significant comparison between the various strategies.

Results from the point-positioning experiments

It is evident from equation (2) that the effect of horizontal gradients diminishes quickly as the elevation angle increases [See also Gardner, 1977, and Davis et al., 1993]. Therefore, to sense the gradients it might be necessary to include low elevation angle observations. At the same time, reducing the elevation angle cutoff too much may result in increased errors from multipath and troposphere mapping function. We chose an elevation angle cutoff of 7° as a reasonable compromise. This choice is supported by Bar-Sever [1996] who reports superior agreement in wet zenith delay estimates between a collocated WVR and a GPS receiver, using this cutoff value, and by MacMillan and Ma [1994] who report improved VLBI baseline length repeatabilities using this cutoff value.

We began with a massive experiment intended to isolate the impact of the gradient model on point positioning by comparing the performance of the nominal inhomogeneous strategy and the nominal homogeneous strategy. in this experiment wc independently point-positioned twice all the available IGS sites during October - December, 1996, for each strategy. For each site we computed the mean

position and velocity vectors, weighted by the formal errors, and the weighted daily repeatabilities in the radial, longitude and latitude components of the position vector around these means. At this point the only quality control measure applied was the rejection of one site, CMBB (part of the BARD network in Northern California), because an 8-cm radial repeatability indicated a serious problem with the receiver/site. The mean improvement in 3D position repeatabilities due to the gradient model was a modest 1.6%, and many sites seem to be effected negatively by the gradient model. Figure 1 reveals a correlation between the performance of the nominal inhomogeneous model and the percentage of low elevat ion angle observat ions. Similar behavior is exhibited by the formal errors of the gradient vector and the position vector. Figure 2 shows the formal errors for the gradient (defined as the RMS of the formal errors for G_N and G_E) as a function of the percentage of measurements between 70 and 15°. Figure 1 also reveals that, on average, the percentage of low elevation observat ions at an IGS site is very low; on] y 7% of al l measurements are taken between 7° and 15°, and only 1.2% between 7° and 10° (compared to theoretical 14% and 5%, respectively, assuming all in view tracking and a uniform distribution of the GPS satellites in the local sky).

The preceding results clearly demonstrate the need for a sufficient number of low elevation angle measurements to realize significant improvement with the gradient model. Subsequent experiments were carried out, therefore, on a subset of stations that meet a minimal criterion for the percentage of low elevation angle measurements. Based on Figure 1, that criterion was chosen to be 2% of the total number of measurement taken between 7° and 10° elevation. Figure 1 shows that most sites satisfying this criterion display improvement in position repeatability. On average, 37 out of the 150 IGS sites that participated in our experiment satisfied this criterion, on average, during October - December, 1996.

We also attempted to improve the performance of the gradient model by tuning the estimation strategy on a small number of sites. The two tuning parameters were the random walk sigma for the gradient parameters and the size of the rejection window for post-fit phase residuals. Figure 3 depicts the tuning process for onc site, AOA 1 (in southern California), that performed rather poorly with the nominal inhomogeneous strategy. The results suggested that our nominal inhomogeneous strategy was sub-optimal. Halving the size of the post-fit phase window and of the random walk sigma from their nominal value gave superior results. 'I'he reduction in post-fit window size is probably an artifact of the increase in the number of degrees of freedom duc to the gradient parameters.

Next, we tested all six strategies in Table 1 on the 37 sites that satisfied the minimum criterion for low elevation measurements. For each estimation strategy and for each site we computed the repeatability in the daily position estimates. 'fable 2 summarizes the mean improvement in position repeatability for each strategy relative to the repeatability obtained with the current JPL strategy. The tuned inhomogeneous strategy proved to bc far superior to the five other tested strategies for this data set in all components of the position vector. The mean improvement in 3D position repeatability was 18.5% relative to the current JPL strategy. Only two sites, STJO (St. John, Canada) and YAR1 (Yaragadee, Australia), experienced small degradation in 3D position repeatability due to the tuned inhomogeneous strategy as compared to the current JPL strategy. The relative improvement for each of the participating sites and for each strategy is given in Table A 1.

The repeatability of the radial component of the position vector improves, on average, when lowering the elevation angle, regardless of the details of the gradient model, in agreement with a number of other studies [13ar-Sever and Kroger, 1996, for GPS, and MacMillan and Ma, 1994, for VLBI]. The presence of the gradient model is seen to improve the radial repeatability even further, and the best repeatabil it ics arc obtained with the tuned inhomogeneous strategy, with average radial repeatability improvement of 19.5%. Only four sites, ONSA(Onsala, Sweden), REYK (Reykjavik,

Iceland), STJO and YAR 1 experienced degradation in the radial position repeatabilities due to the tuned inhomogeneous strategy.

The horizontal component of the estimated position vector behaves markedly differently than the radial component. Table 2 demonstrates that a reduction in elevation angle cutoff value without the additional estimation of a troposphere gradient will tend to degrade the repeatability of the horizontal components. The best results arc, again, obtained with the tuned inhomogeneous strategy. It is noteworthy that the repeatability of the horizontal component of the position vector using the tuned 15° strategy was superior to all other strategies, except the tuned inhomogeneous strategy.

Bar-Sever and Kroger [1996] have shown that the choice of elevation angle cutoff value effects the mean of the radial component oft he cst i mated position vector, as well as its scatter. Indeed, Table 3 reveals that significant radial biases arc associated with the change of elevation angle cutoff. The presence of the gradient model tends to reduce the bias associated with elevation angle cutoff by about 25%. The impact of the gradient model on the biases in the horizontal coordinates is larger than that of the elevat ion angle cutoff val UC, but both are very smal 1. There are too few southern hemisphere sites in our experiments to form a meaningful distinction between their response to the various strategies and the response of the northern hemisphere sites.

Comparison between GPS and WVR wet zenith delay estimates

The next set of experiments were designed to gauge the impact of the gradient model on the GPS solution through an independent evaluation of an important GPS product, namely, the Zenith Wet Delay (ZWD). Such evaluat ions have been carried out extensively by many researchers, as an effort to validate the GPS-based estimates for meteorological appl icat ions. The Water Vapor Radiometer (WVR) has been the primary tool in these evaluations due to its high level of precision and because it

is considered a more established technology for the retrieval of ZWD [Bar-Sever, 1996, Businger et al., 1996, Duan et al. 1996, Runge et al., 1995, Wolfe and Gutman, 1994, Elgered et al., 1995, Rocken et al., 1995, Chiswell and Businger, 1995]. We were able to carry out a ZWD comparisons between a GPS receiver and a WVR at two sites, GOL3 (Goldstone, California) and ONSA (Onsala, Sweden. Scc the next section for more information about this WVR). The comparison at GOL3 spanned 30 days in July, 1996, and the comparison at ONSA spanned 28 days in October, 1995. The GOL3 receiver had a moderate number of low elevation observations during the experiment: 1.2% between 7° anti 10°, and 7.7% between 7° and 15°. The ONSA receiver is consistently better in that regard (see next section). For each of these sites we had available precise measurements of surface pressure, which enabled us to extract the ZWD from the TZD. Each site was point-positioned daily using three estimation strategies: the current JPL strategy, the nominal homogeneous strategy and the tuned inhomogeneous strategy. The results of the comparisons are summarized in Table 4. As Table 4 indicates, a reduction in scatter around the mean is associated with the lowering of elevation angle cutoff for GPS observations, and is a well known phenomenon [Bar-Sever, 1996, Runge et al., 1995]. Most importantl y, Table 4 links the gradient model to a significant additional reduction in the scatter around the mean of the WVR-GPS differences. The tuned inhomogeneous strategy is shown to yield the best agreement with the WVR for both sites.

Direct evaluation of the gradient estimates

While it is clear that employing the troposphere gradient model as part of the tuned inhomogeneous strategy improves the quality of the GPS solution, the reasons for this improvement are uncertain. The simplest explanation is that the gradient model was able to absorb actual tropospheric inhomogeneities. This must be verified before the estimated gradients can be used in meteorological applications. in this section wc present some evidence that strongly supports this explanation. We do so by comparing GPS-based estimates of troposphere gradients to those based on a collocated

WVR. Since water vapor varies on small spatial scales, the WVR and the GPS receiver must be in close proximity. To serve our purposes, the GPS has to track low elevation angles well, and the WVR has to observe a broad range of azimuth and elevation angles. The WVR retrieval algorithm must be well calibrated. Opportunist ics to compare GPS and WVR measurements are very limited as a result of these stringent requirements. Fortunately, such opportunity exists at Onsala, Sweden, where a WVR is located less than 10 m away from the lGS receiver, ONSA. This GPS receiver is one of best in terms of tracking low elevation observations (see table A 1).

Zenith-equivalent of WVR-based line-of-site estimates of wet delay during October, 1995, were kindly supplied by Per Jarlemark from the Onsala Space Observatory. They consist of approximately 6500 measurements per day at 14 uniformly spaced azimuth angles, and at 7 elevation angles, spanning the range from 21.4° to 90°. Altogether, there are 37 distinct az-el pairs. During October 1995, the average fraction of measurements from the ONSA GPS receiver taken between 7° and 10° was 5.8% and between 7° and 15° was 15.3%.

We point-positioned the ONSA receiver during each day in October 1995 using our tuned inhomogeneous strategy. This resulted in a time series of gradient components, G_N and G_E, spanning the whole month of October, with an interval of 5 minutes. Since the WVR does not produce gradient estimates directly, they were derived from the line-of-site observations as follows. We linearly interpolated all the measurements to a common time series such that the interpolation step size was always less than 5 minutes and such that at each interpolated time point all the 37 distinct az-el measurements were available. This resulted in a data set consisting of 2198 time points. At each time point wc have 37 measurements of wet delay at different azimuth and elevation pairs. For each time point wc used the 37 measurements as left-hand-side observations in equation (2), and estimated the gradient vector together with the ZWD in a least squares formalism. This process is analogous to the GPS solution process where several distinct line-of-site observations are combined in time and space to form the estimate of the gradient. To compare the WVR-based estimates with

the. GPS-based estimates wc interpolated the GPS based estimates to the WVR time series. Since GPS estimates are given every 5 minutes, the interpolation step size is always less than 5 minutes. The WVR-based estimates of ZWD that were used in the comparison with the GPS-based estimates, above, were derived by this process. The excellent agreement with the GPS-based estimates of ZWD, reported in Table 4, offers some validation for this approach.

The formal errors of the GPS- and WVR-based gradient estimates are summarized in table 5 and the corresponding uncertainties in the magnitude and azimuth of the vectors are illustrated in Figure 4. The WVR-based estimates arc formally more accurate than the GPS-based estimates by a factor of 5.

At this point, the GPS-based gradients arc not likely to compare well with the WVR-based gradients. This is because the GPS-based gradients include a hydrostatic component that is absent from the WVR data. Because the hydrostatic gradient varies, typically, on a much longer time scale than the wet gradient [Davis et al., 1993, MacMillan, 1995], wc might be able to remove it using independent observations, from objective anal ysis, or from a local climatology of the hydrostatic gradient. To simulate this approach, wc assumed that the hydrostatic gradient changes on a 12-hour scale. We partitioned the data set into 12-hour segments, centered on local noon and midnight, and we "de-biased" the GPS-based gradient estimates at each segment with respect to the WVR-based gradients. That is, the mean difference between the GPS-based gradient and the WVR-based gradient during each segment was removed. This also enabled us to include all the segments in one data set. We further restricted our data set to those 12-hour segments that contain measurements at least every 15 minutes. This final data set contained 20 12-hour segments and 1374 points. The hydrostatic gradients extracted in this way arc presented in Figure 5. A prevailing hydrostatic gradient, roughly in the north-south direction and 0.06 cm in magnitude is observed. The month-long mean in the GPS total delay gradient had a magnitude of 0.03 cm and azimuth of 194° (that translates to a delay of 9.8 mm at 10° elevation, and agrees quit well with the 3 years mean total

gradient of 10.2 mm and 164° azimuth estimated by Chen and Herring [1997] using the Onsala VLB1). The monthly mean wet gradient, as observed by the WVR, has a similar magnitude, but an azimuth of 45°, approximately. The similarity in magnitude of the mean hydrostatic gradient and wet gradient hampers our ability to separate these components based on long-term averages, and highlights the need to fold in independent observations of the hydrostatic gradient.

Figure 6 illustrates the correlation between the GPS-based wet gradient estimates and the WVR-based estimates in terms of the magnitude of the vectors. The linear correlation between the GPS-based magnitude and the WVR-based magnitude is 0.56, which is significant at the 100% level (i.e. very unlikely to be a random occurrence). The slope of the linear fit, displayed in Figure 5, tends to get closer to 1 when large gradients are excluded from the fit, but that causes the linear correlation to degrade (Table 6). Table 6 reveals that the GPS-based gradients systematically differ from the WVR-based gradients by about 60%. For large gradients, this discrepancy is due to the GPS-based magnitudes being uniformly smaller than the WVR-based magnitudes. For weaker gradients, the discrepancy appears to be noisy. in contrast, the two technologies display a remarkable agreement in the azimuth of the gradient vector, with better than 10° agreement for strong gradients (larger than 0.2 cm in magnitude). The agreement in azimuth improves as the gradient magnitudes get larger as is illustrated in Figure 7. Finally, a sample of wet gradient estimates from each technology is depicted in Figure 8, showing good correlation between the two solutions.

Discussion

In the first part of this paper wc demonstrated that utilization of the troposphere gradient model with a proper estimation strategy leads to improvements in precision and accuracy for precise point positioning. The improvement in precision is inferred from a significant reduction in position repeatabilities. The improvement in accuracy is inferred from direct comparisons of ZWD estimates with the independent technique of water vapor radiometry. Although the improvement appears to be robust it can vary considerably from site to site. Of particular concern are the four sites (ONSA, REYK, STJO and YAR1) that seem to be adversel y affected by the presence of the gradient model. An inspection of l'able A 1 reveals that it is not the presence of the gradient model that causes a degradation in repeatability compared to the current JPL estimat ion strategy but, rather, the reduction in elevation angle cutoff value. For these sites (and for almost all other tested sites) the tuned inhomogeneous strategy is far superior to the nominal homogeneous strategy. At low elevation angles the impact of the gradients on the observable becomes very significant and prevailing gradients will have systematic effects on the estimation of geodetic quantities. The emerging rule is that a reduction in elevation angle cutoff value from 15° or 20° to the 5° - 10° range, should be accompanied by modeling the troposphere gradient, especially if good horizontal repeatability is desired.

Variants of the constant gradient strategy were employed by MacMillan [1995] for VLBI data processing. Wc tested this strategy in order to provide an alternative strategy for those who do not use stochastic models. This strategy could be employed to observe the hydrostatic gradient in the troposphere, but it is clearly unsuitable for the observation of moisture gradients because of their short time scales. Overall, this strategy proved an able performer, although on average, it is inferior to the tuned inhomogeneous strategy. The full performance statistics are provided in table A 1. Obviously, site-specific tuning of estimation strategy and mapping function will provide the best

performance, but a non-uniformity of the estimation strategy would probably not be tolerated in most operational processes.

Many factors contribute to the variety of responses to the tuned estimation strategy. At this time we can only speculate that factors such as local multipath and phase center pattern may effect the results in an unpredictable way. We note that the ONSA GPS antenna is covered with a radome and that the data for our experiments were collected during the northern hemisphere winter, when snow and ice can effect the phase pattern of the GPS antenna at some sites. Some antennae are more noisy at low elevation angles than others, etc. The study of errors introduced by the simple mapping function we employed here might be an interesting and fruit ful invest igat ion. For example, Chen and Herring [1997] proposed an inhomogeneous mapping function that should be more accurate than (2), especially at low elevation angles.

Biases associated with the change of elevation angles cutoff arc unavoidable, for most receivers. We have contributed here one more piece of evidence (to an already large collection) linking the reduction in elevation angle cutoff to improved accuracy (Tables 2 and 4). It is noteworthy that the presence of the gradient model tends to reduce these biases.

Note: recent analysis carried out at JPL found that the estimation of atmosphere gradients with the tuned 15° strategy at all the sites participating in the global determination of GPS orbits and clocks resulted in 10% improvement to the median orbit repeatabilities of all satellites. The tuned inhomogeneous strategy gave essentially the same results because most IGS sites do not track well below 15°. As a result, starting August 24, 1997, the IGS Analysis Center at JPL has switched its estimation strategy for the global solution and for point-positioning to the tuned 15° strategy [IGS, 1997]

The second part of this paper is dedicated to the validation of a new GPS product: estimates of troposphere gradients. We have shown that GPS-based estimates of troposphere gradients seem to capture accurately the direction (azimuth) of significant moisture gradients. The magnitude of the gradients is captured less accurately, with errors at the 60% level. The primary error source in our data processing is the crude treatment of the hydrostatic delay which, of course, does not remain exactly constant over contiguous 12-hour intervals. This must be a major contributor to the large difference in magnitude between the GPS- and the WVR-based gradients. Another major error source is the inability of the GPS estimates to track fast-changing gradients due to the tight time correlation imposed by the random walk sigma of 10"9 cm/√sec. Relaxing the random walk sigma results, typically, in improved agreement in magnitude of large gradients with the WVR, but at the cost of lower linear correlation overall and increased discrepancy in azimuth.

Errors in our method to extract gradient estimates from the line-of-sight WVR delay could also have contributed to degradation in the comparison statistics. In particular, the relatively high elevation angle cutoff of the WVR observations may have effected the accuracy of the retrieval. It also implies that the GPS senses a rather different atmosphere than the WVR does. An increase in the GPS elevation angle cutoff to 15° did not improve the agreement. Site-specific error sources, such as multipath and antenna characteristics, may be another factor that strongly impacts our comparison. The inhomogeneous mapping function, $m_\Delta(e)$ cot e, may also introduce significant errors at low elevation angles, as indicated by Chen and Herring [1997]. A systematic error may be present in the GPS solution due to the azimuthally asymmetric distribution of observations (Figure 9), especially in light of the fact that the dominant gradients, as observed by the WVR are in the north-south direction (Figure 10), and the consequent dominance of the G_N component of the gradient relative to G_E (Figure 8). However, the similarity in formal errors between the two GPS-based gradient

components and the good agreement in azimuth with the WVR-based gradients, suggest no ill effects on the GPS estimates due to this asymmetry.

It is important that future comparisons will bc carried out at other sites in order to construct a reliable error budget for the cst i mat ion oft roposphere gradients. An alternative method for the validation of the GPS gradient estimate is to deploy a dense network of GPS receivers around the test receiver, and use the ZWD from each receiver to construct the local wet delay field. We expect the ability to retrieve troposphere gradients to improve as ncw receivers and antennae are designed to produce high quality observations at low elevation angles.

Appendix

Table Al. Point positioning statistics for the 37 sites on which five estimation strategies were tested. Percent improvement is measured relative to the current JPL strategy. Therefore, a positive number indicates improvement over this strategy and a negative number indicates degradation.

Column legend

%15 - percent of measurements taken below 15°.

%10 - percent of measurements taken below 100.

%rad - percent improvement in repeatabilit y of the radial component of the position vector,

%lat - percent improvement in repeatabilit y of the latitude component of the position vector.

%lon - percent improvement in repeatability of the longitude component of the position vector.

%2D - percent improvement in repeatabilit y of the horizontal component of the position vector

(= √(%lat^2 + %1011)).

%3D - percent improvement in the position vector (= √(%rad^2 + %lat^2 + %lon^2)).

%chi- percent improvement in Chi Square of position vector.

rad - repeatabi 1 it y, in cent imctcrs, of the radial component of the position vector.

lat - repeatabil it y, in centimeters, oft he lat it udc component of the position vector.

Ion - repeatability, in centimeters, of the longitude component of the position vector.

= current JPL estimation strategy

* = nominalhomogeneous estimation strategy

& = constant gradient estimation strategy

/ = nominal inhomogeneous estimation strategy

% = tuned 15° strategy

+ = tuned inhomogeneous estimation strategy

All comparisons are done with respect to current JPL estimation strategy

SITE	%15	%10	%rad	%lat	%lon	%2D	%3D	%chi	rad	lat	1 on
AOA1									1.22	0.32	0.48
AOA1 *	8.71	2.21	28.93	-2.11	-4.88	-4.02	21.89	-30.81	0.87	0.33	0.50
AOA 1 &	8.71	2.21	35.32	-3.32	-6.47	-5.49	26.69	-8.06	0.79	0.33	0.51
AOA1 /	8.81	2.27	22.2.8	-3.26	-1.74	-2.22	17.28	11.71	0.95	0.33	0.49
AOA1 %	0	0	21.51	4.69	17.60	13.33	20.04	55.38	0.96	0.30	0.40
AOA1 +	8.04	1.88	40.99	15.55	20.73	19.08	36.44	42.78	0.72	0.27	0.38
ASC1									1.24	0.51	1.06
ASC1 *	13.11	3.11	0.23	-4.81	-1.30	-1.97	-0.83	-39.69	1.24	0.53	1.07
ASC1&	13.11	3.11	2.64	-4.51	0.88	-0.21	1.29	-7.39	1.21	0.53	1.05
ASC1 /	13.12	3.11	8.95	-4.40	1.04	-0.01	4.58	26.40	1.13	0.53	1.05
ASC1 %	0	0	-6.59	-3.89	2.39	1.11	-3.03	46.00	1.32	0.53	1.03
ASC1+	12.73	3.02	6.80	-3.25	4.14	2.70	4.83	19.28	1.16	0.53	1.02
AUCK									0.96	0.51	0.69
AUCK*	10.77	2.62	-3.44	-5.89	0.38	-1.92	-2.77	-45.41	0.99	0.54	0.69
AUCK&	10.77	2.62	8.17	6.50	3.41	4.49	6.50	-1.47	0.88	0.48	0.67
AUCK/	10.90	2.70	13.02	7.64	3.54	5.00	9.37	24.96	0.84	0.47	0.67
AUCK%	0	0	7.22	10.60	9.32	9.77	8.35	53.46	0.88	0.46	0.63
AUCK+	10.53	2.61	14.12	10.95	6.85	8.31	11.50	22.79	0.82	0.45	0.64
BOR1									0.70	0.45	0.58
BOR1*	6.75	2.06	10.56	-3.90	0.40	-1.22	4.20	-23.16	0.63	0.47	0.58
BOR1&	6.75	2.06	8.50	12.26	6.39	8.46	8.48	20.84	0.64	0.39	0.54
BOR1/	6.78	2.08	9.55	12.02	6.48	8.49	9.00	40.09	0.63	0.40	0.54
BOR1 %	0	0	5.53	23.69	30.32	27.86	16.64	67.08	0.66	0.34	0.40
BOR1 +	6.65	2.04	16.60	19.15	33.10	27.62	22.18	51.86	0.58	0.36	0.39
CAGL									0.79	0.41	0.51
CAGL*	9.33	3.03	14.67	-13.62	-0.20	-5.77	5.82	-55.09	0.67	0.47	0.51
CAGL&	9.33	3.03	5.66	5.75	2.02	3.46	4.77	-4.89	0.75	0.39	0.50
CAGL/	9.41	3.09	17.79	7.81	0.81	3.54	11.72	25.92	0.65	0.38	0.51
CAGL%	0	0	10.91	11.11	14.17	12.96	11.73	56.26	0.70	0.36	0.44
CAGL+	8.98	2.94	12.54	11.74	4.64	7.41	10.42	22.74	0.69	0.36	0.49
CIT1									1.10	0.35	0.48
CIT1*	9.17	2.16	13.97	-6.96	-1.82	-3.61	9.72	-50.04	0.95	0.37	0.49
CIT1&	9.17	2.16	20.73	-0.46	-1.73	-1.30	15.67	-9.31	0.87	0.35	0.49
CIT1/	9.20	2.17	19.12	-2.10	-0.46	-1.02	14.18	17.52	0.89	0.36	0.48
CIT1%	0	0	34.17	24.78	23.48	23.92	31.91	68.14	0.72	0.26	0.37
CIT1+	9.12	2.15	34.60	23.71	22.12	22.66	31.73	46.19	0.72	0.27	0.37

Coco									1.91	0.74	0.86
COCO*	13.97	3.85	12.41	-4.30	-6.56	-5.60	7.38	-42.72	1.67	0.77	0.92
COCO&	13.97	3.85	20.75	9.27	6.04	7.37	17.15	18.37	1.51	0.67	0.81
COCO/	14.86	4.42	12.95	10.96	-2.21	3.18	10.30	24.61	1.66	0.66	0.88
COCO%	0	0	4.68	-8.32	5.25	-0.62	3.31	47.55	1.82	0.80	0.81
COCO+	13.33	3.56	22.33	3.17	10.02	7.04	18.07	30.40	1.48	0.72	0.77
FARB									1.25	0.35	0.53
FARB *	15.71	5.68	11.48	-23.15	-11.59	-15.25	5.25	-110.53	0.31	0.65	0.00
FARB&	15.71	5.68	24.29	-0.79	3.08	1.87	19.21	-19.48	0.95	0.35	0.51
FARB /	15.91	5.81	24.6'7	-2.62	3.14	1.34	19.23	6.19	0.94	0.36	0.51
FARB%	0	0	19.53	6.06	12.26	10.31	17.56	56.63	1.01	0.33	0.47
FARB+	15.70	5.74	38.95	23.21	24.14	23.86	35.49	38.82	0.76	0.27	0.40
FORT									1.36	0.52	0.83
FORT '	14.16	4.19	23.25	-9.35	12.57	5.81	16.86	-52.48	1.04	0.57	0.73
FORT&	14.16	4.19	25.0"1	5.87	7.70	7.17	18.85	23.30	1.02	0.49	0.77
FORT /	14.40	4.30	22.75	3.28	4.16	3.91	15.81	42.73	1.05	0.50	0.80
FORT%	0	0	9.38	2.93	-0.46	0.51	6.42	61.89	1.23	0.50	0.83
FORT+	13.42	3.99	27.72	4.92	7.00	6.40	19.77	42.32	0.98	0.49	0.77
GRAS									0.92	0.37	0.42
GRAS*	12.10	3.33	20.42	-6.47	-5.84	-6.11	12.40	-48.67	0.73	0.39	0.44
GRAS &	12.10	3.33	23.47	0.59	-0.89	-0.25	16.60	-15.74	0.70	0.37	0.42
GRAS /	12.20	3.41	26.55	0.95	-6.97	-3.63	17.24	10.97	0,68	0.37	0.45
GRAS%	0	0	12.7'?	3.30	6.51	5.11	10.69	48.01	0.80	0.36	0.39
GRAS+	10.98	2.98	25.57	3.90	7.94	6.18	19.83	12.30	0.68	0.36	0.39
HBRK									0.85	0.31	0.60
HBRK*	11.55	2.27	-3.36	-5.84	8.55	5.33	-0.06	-49.26	0.88	0.33	0.55
HBRK&	11.55	2.27	-0.89	7.55	24.47	20.78	7.33	-0.08	0.86	0.29	0.45
HBRK/	11.64	2.32	-1.65	10.20	13.59	12.86	3.75	16.11	0.86	0.28	0.52
HBRK%	0	0	-0.47	18.46	33.19	29.98	10.68	61.99	0.85	0.25	0.40
HBRK+	11.09	2.17	9.34	25.57	34.00	32.14	17.48	39.95	0.77	0.23	0.40
HKLO									0.99	0.31	0.70
HKLO*	11.95	2.01	15.07	-8.02	3.28	1.31	9.67	-46.31	0.84	0.33	0.68
HKLO&	11.95	2.01	26.12	2.21	11.24	9.72	19.35	-2.73	0.73	0.30	0.62
HKLO/	12.07	2.07	12.50	0.54	17.19	14.21	13.13	17.99	0.87	0.31	0.58
HKLO%	0	0	3.63	26.06	22.00	7.96	51.78	37.63	0.95	0.23	0.55
HKLO+	11.32	1.98	18.91	19.74	30.58	28.67	22.43	37.63	0.80	0.25	0.49
HOPB									1.25	0.37	0.59
HOPB*	16.54	6.10	13.16	-17.67	-2.24	-6.95	8.00	-103.86	0.32	0.69	0.00
HOPB&	16.54	6.10	17.52	-4.33	3.72	1.33	13.58	-37.76	1.03	0.39	0.57
HOPB/	16.71	6.23	19.40	1.28	7.31	5.52	15.91	1.69	1.01	0.37	0.55
HOPB%	0	0	13.11	4.49	19.56	14.93	13.52	54.35	1.09	0.35	0.47
HOPB+	16.45	6.12	29.22	12.81	20.20	17.99	26.40	19.46	0.88	0.32	0.47

KELY									0.99	0.34	0.57
KELY*	10.41	2.62	21.47	-15.30	-4.98	-7.80	11.35	-64.15	0.78	0.39	0.60
KELY&	10.41	2.62	17.42	1.37	9.28	7.18	14.17	-25.40	0.82	0.34	0.52
KELY/	10.44	2.62	18.09	2.95	9.46	7.70	14.73	11.66	0.81	0.33	0.52
KELY%	O	0	14.47	5.43	15.08	12.49	13.86	42.81	0.85	0.32	0.48
KELY+	10.26	2.62	21.79	12.91	19.96	18.04	20.61	18.87	0.″17	0.30	0.46
KWJ 1									2.02	0.59	1.07
KWJ1 *	13.54	3.37	20.86	-10.20	-3.03	-4.74	13.25	-41.13	1.60	0.65	1.10
KWJ 1 &	13.54	3.37	24.53	22.93	0.32	4.75	18.75	23.77	1.52	0.45	1.07
KWJ 1 /	14.01	3.58	27.81	22.53	-0.97	3.97	20.71	47.00	1.46	0.46	1.08
KWJ1%	O	0	15.65	22.22	11.50	13.70	15.12	63.43	1.70	0.46	0.95
KWJ 1 +	12.11	3.14	30.83	28.93	4.96	9.95	24.66	51.38	1.40	0.42	1.02
LMNO									0.87	0.35	0.61
LMNO *	12.62	2.53	10.32	-7.48	7.34	3.49	7.55	-45.12	0.78	0.38	0.57
LMNO&	12.62	2.53	14.21	-2.02	15.25	10.84	12.80	-8.42	0.75	0.36	0.52
LMNO /	12.72	2.58	15.67	1.43	16.89	12.84	14.54	18.08	0.-13	0.34	0.51
LMNO%	O	0	2.42	4.50	24.20	19.08	8.97	51.79	0.85	0.33	0.46
LMNO+	12.21	2.44	17.35	14.10	25.96	22.89	19.50	30.08	0.72	0.30	0.45
METS									0.73	0.28	0.50
METS *	13.93	4.15	8.15	-6.70	9.57	5.46	7.12	-47.77	0.67	0.30	0.45
METS&	13.93	4.15	9.72	-0.49	22.11	16.42	12.27	-11.97	0.66	0.28	0.39
METS/	13.96	4.17	14.60	-0.91	-0.26	-0.42	8.63	2.09	0.62	0.28	0.50
METS%	O	0	1.36	-4.92	29.21	20.14	8.21	49.47	0.72	0.29	0.35
METS+	13.93	4.16	16.07	3.59	21.28	16.74	16.32	12.01	0.61	0.27	0.39
MOIN									1.79	0.55	1.11
MOIN*	14.05	3.25	-0.73	-17.97	-2.80	-5.99	-2.46	-61.91	1.80	0.65	1.14
MOIN&	14.05	3.25	2.83	16.99	-5.37	-1.18	1.55	7.94	1.72	0.46	1.17
MOIN/	14.54	3.45	19.56	14.55	-1.27	1.67	13.38	39.34	1.44	0.47	1.12
MOIN%	O	0	11.13	15.26	2.64	5.09	9.19	56.82	1.59	0.47	1.08
MOIN+	13.48	3.17	12.08	25.34	10.04	12.87	12.33	46.23	1.57	0.41	1.00
0AT2									1.07	0.41	0.53
0AT2 *	11.13	3.37	5.95	-13.22	-9.11	-10.66	0.96	-84.33	1.01	0.46	0.58
0AT2 &	11.13	3.37	11.58	1.56	-9.20	-5.27	6.84	-22.96	0.95	0.40	0.58
0AT2 /	11.19	3.41	8.49	5.64	-3.07	0.09	6.03	12.97	0.98	0.39	0.55
0AT2%	o	0	20.20	24.54	18.43	20.68	20.32	66.11	0.85	0.31	0.43
0AT2 +	10.93	3.34	24.14	18.86	21.68	20.61	23.13	34.73	0.81	0.33	0.42
OBER									0.77	0.24	0.44
OBER*	11.77	3.62	17.51	-13.99	4.24	-0.26	11.90	-52.33	0.64	0.27	0.42
OBER&	11.77	3.62	24.81	4.13	9.31	8.13	19.32	-8.56	0.58	0.23	0.40
OBER/	11.80	3.63	12.48	4.25	-8.22	-5.47	6.83	2.00	0.67	0.23	0.48
OBER%	O	0	2.38	16.84	0.90	4.23	2.94	37.75	0.75	0.20	0.44
OBER+	11.60	3.60	16.71	14.24	8.12	9.50	14.52	13.50	0.64	0.21	0.40

ONSA									0.64	0.32	0.41
ONSA*	14.89	5.70	-11.50	-10.70	-13.55	-12.45	-11.88	-84.94	0.71	0.35	0.47
ONSA&	14.89	5.70	-4.74	-2.17	-0.81	-1.34	-3.40	-35.24	0.67	0.33	0.41
ONSA/	14.93	5.73	-7.79	-1.74	-4.71	-3.57	-6.13	-6.02	0.69	0.33	0.43
ONSA%	0	0	9.76	0.40	8.49	5.27	7.94	49.25	0.58	0.32	0.38
ONSA+	14.49	5.55	-2.36	1.61	10.86	7.16	1.33	-2.41	0.66	0.31	0.37
PLTC									0.85	0.30	0.48
PLTC *	12.67	3.16	10.05	-0.60	-1.42	-1.19	6.70	-46.71	0.80	0.30	0.49
PLTC&	12.6"1	3.16	12.22	-10.56	-2.10	-4.55	7.12	-31.10	0.18	0.33	0.49
PLTC /	12.75	3.17	11.47	-6.92	1.68	-0.82	7.79	-1.11	0.79	0.32	0.47
PLTC%	0	0	17.74	1.5.20	16.35	16.02	17.24	58.66	0.73	0.25	0.40
PLTC+	12.06	3.00	22.19	16.84	19.05	18.42	21.10	28.77	0.69	0.25	0.39
POL2									0.70	0.54	0.73
POL2 *	10.19	2.44	10.07	-2.41	3.25	1.19	4.39	-34.08	0.63	0.55	0.71
POL2&	10.19	2.44	14.07	-2.56	1.67	0.14	5.08	1.52	0.60	0.55	0.72
POL2 /	10.20	2.45	9.11	0.79	-0.44	-0.00	3.28	23.08	0.64	0.54	0.73
POL2 %	0	0	-0,90	0.17	1.63	1.11	0.36	48.57	0.71	0.54	0.72
POL2 +	10.14	2.41	11.94	0.96	6.94	4.76	7.36	19.92	0.62	0.53	0.68
REYK									0.84	0.30	0.47
REYK*	12.35	3.46	-5.66	-35.69	-2.45	-12.99	-7.92	-114.80	0.32	0.64	0.00
REYK&	12.35	3.46	-5.46	17.08	10.30	12.19	-0.47	-19.36	0.89	0.25	0.42
REYK/	12.38	3.49	-0.95	14.01	14.36	14.26	3.38	10.79	0.85	0.26	0.40
REYK%	0	0	7.05	13.40	14.44	14.14	9.13	51.45	0.78	0.26	0.40
REYK+	12.01	3.45	-2.64	19.18	22.66	21.65	4.03	8.02	0.86	0.24	0.36
SPK1									1.25	0.33	0.58
SPK1*	9.73	2.45	23.32	1.29	-6.18	-4.44	16.41	-39.69	0.96	0.33	0.62
SPK1&	9.73	2.45	17.11	-1.47	-3.74	-3.20	12.23	-18.57	1.04	0.33	0.60
SPK1 /	9.77	2.47	18.86	4.45	-8.44	-5.50	12.91	6.06	1.01	0.32	0.63
SPK1%	0	0	19.68	16.91	20.68	19.76	19.70	57.87	1.00	0.27	0.46
SPK1+	9.34	2.38	33.66	21.09	16.94	17.92	29.89	35.29	0.83	0.26	0.48
STJO									0.87	0.37	0.58
STJO*	13.95	4.82	-28.95	-14.60	-3.93	-7.15	-20.96	-97.35	1.12	0.42	0.60
STJO&	13.95	4.82	-30.21	0.51	4.98	3.65	-18.22	-43.77	1.13	0.37	0.55
STJO/	14.06	4.90	-11.99	-1.58	8.60	5.51	-5.54	2.57	0.97	0.38	0.53
STJO%	0	0	3.21	1.26	17.74	12.61	6.75	51.95	0.84	0.37	0.48
STJO+	13.65	4.79	-10.36	11.97	18.09	16.26	-0.86	7.17	0.96	0.33	0.48
THU1									0.93	0.27	0.32
THU1 *	10.53	2.23	17.52	-13.59	-20.97	-17.92	10.63	-89.45	0.77	0.31	0.39
THU1 &	10.53	2.23	26.51	-11.44	1.83	-3.96	20.61	-19.27	0.68	0.30	0.31
THU1 /	10.57	2.25	27.60	-12.14	6.15	-1.94	21.89	4.22	0.67	0.30	0.30
THU1 %	0	0	8.37	-5.04	10.09	3.44	7.53	42.90	0.85	0.28	0.29
THU1+	10.03	2.13	29.55	-8.96	12.96	3.14	24.50	7.31	0.66	0.29	0.28

TIBB									1.28	0.35	0.61
TIBB*	8.94	3.23	-6.62	-9.15	-2.61	-4.29	-6.08	-77.31	1.36	0.38	0.63
TIBB&	8.94	3.23	8.58	-11.32	3.25	-0.60	6.35	-2.79	1.17	0.39	0.59
TIBB/	9.02	3.29	17.92	-1.07	10.07	7.15	15.27	27.99	1.05	0.35	0.55
TIBB%	O	0	12.64	-29.26	13.27	0.87	9.75	40.15	1.12	0.45	0.53
TIBB+	8.66	3.03	26.75	0.11	21.52	15.64	24.00	34.85	0.94	0.35	0.48
TMGO									1.00	0.34	0.51
TMGO *	10.34	2.15	9.9'2	0.39	1.47	1.14	7.46	-40.36	0.90	0.34	0.50
TMGO&	10.34	2.15	10.27	2.54	-0.04	0.73	7.60	-11.30	0.90	0.33	0.51
TMGO /	10.40	2.18	7.46	3.28	3.73	3.59	6.40	11.47	0.93	0.33	0"49
TMGO%	O	0	8.78	10.50	27.14	21.73	12.09	58.54	0.91	0.30	0.37
TMGO+	9.95	2.05	20.78	25.41	23.90	24.35	21.73	38.83	0.79	0.25	0.39
TROM									1.14	0.56	0.58
TROM *	9.51	2.37	16.66	-6.06	4.13	-0.89	10.36	-42.53	0.95	0.59	0.56
TROM&	9.51	2.37	21.13	3.69	-0.43	1.53	14.02	-9.70	0.90	0.54	0.58
TROM /	9.61	2.40	16.77	3.76	-3.01	0.18	10.83	10.14	0.95	0.54	0.60
TROM%	O	0	16.53	3.26	5.94	4.64	12.34	45.37	0.95	0.54	0.55
TROM+	9.15	2.28	25.66	10.71	12.19	11.47	20.59	22.78	0.85	0.50	0.51
USUD									0.99	0.49	0.81
USUD*	7.47	2.07	7.82	-0.26	-1.48	-1.15	3.40	-24.18	0.91	0.49	0.82
USUD&	7.47	2.07	-6.82	-0.43	1.54	1.01	-3.13	1.69	1.06	0.49	0.80
USUD/	7.49	2.09	-3.13	3.50	3.29	3.35	-0.06	26.92	1.02	0.47	0.78
USUD%	O	0	1.55	-0.47	7.46	5.26	3.32	49.14	0.97	0.49	0.75
USUD+	7.37	2.06	0.22	2.72	6.91	5.77	2.85	21.04	0.99	0.48	0.75
WEST									1.12	0.31	0.60
WEST*	10.73	2.72	3.51	-10.74	-5.83	-6.88	0.62	-71.85	1.08	0.34	0.63
WEST&	10.73	2.72	5.53	2.25	-1.71	-0.89	3.77	-32.20	1.06	0.30	0.61
WEST/	10.78	2.74	10.67	11.35	0.03	2.30	8.35	9.44	1.00	0.27	0.60
WEST%	O	0	28.14	1.70	19.16	15.19	24.46	54.55	0.80	0.30	0.49
WEST+	10.66	2.71	28.31	14.30	19.26	18.19	25.47	27.90	0.80	0.27	0.48
WHC1									1.10	0.33	0.52
WHC1 *	9.77	2.78	20.23	-4.25	-3.87	-3.98	13.81	-45.74	0.88	0.34	0.54
WHC 1 &	9.77	2.78	15.68	-6.23	-7.15	-6.88	9.76	-26.49	0.93	0.35	0.56
WHC1 /	9.83	2.82	18.63	-1.95	1.08	0.18	13.85	10.74	0.90	0.34	0.51
WHC1%	O	0	22.13	7.40	12.02	10.64	19.23	56.24	0.86	0.31	0.46
WHC1+	9.67	2.77	33.22	17.49	21.58	20.36	29.93	36.60	0.73	0.27	0.41
WHI1									1.06	0.34	0.53
WHI1*	9.77	2.54	14.35	-5.30	-4.38	-4.65	8.95	-47.67	0.91	0.36	0.55
WHI1&	9.77	2.54	16.42	1.06	-7.75	-5.29	10.18	-9.85	0.89	0.34	0.57
WHI1/	9.82	2.57	17.59	-0.44	-4.12	-3.07	11.67	14.21	0.87	0.34	0.55
WHI1%	O	0	21.93	15.27	16.83	16.38	20.43	61.88	0.83	0.29	0.44
WHI1+	9.48	2.52	32.56	19.89	19.81	19.83	28.98	41.28	0.71	0.27	0.43

YAR1									0.76	0.24	0.46
YAR1*	10.93	3.13	-7.02	-10.41	-2.08	-3.89	-6.04	-70.81	0.81	0.26	0.47
YAR1&	10.93	3.13	-2.94	-13.32	-2.51	-4.89	-3.56	-45.81	0.78	0.27	0,47
YAR1 /	10.97	3.16	-2.27	-13.20	-1.03	-3.71	-2.73	-9.68	0.78	0.27	0.46
YAR1%	0	0	1.23	-10.3[)	-4.92	-6.09	-1.15	32.66	0.”15	0.26	0.48
YAR1 +	10.78	3.09	-0.65	-11.38	--1.33	-3.53	-1.57	-20.52	0.76	0.27	0.47
YELL									0.89	0.20	0.34
YELL*	12.22	2.38	7.04	-10.04	-2.59	-4.65	5.03	-79.53	0.83	0.22	0.35
YELL&	12.22	2.38	5.96	-10.58	5.15	0.66	5.07	-48.19	0.84	0.22	0.32
YELL /	12.23	2.39	10.05	-14.60	1.40	-3.16	7.76	-14.77	0.80	0.23	0.34
YELL%	0	0	13.59	1.22	10.24	7.72	12.61	42.49	0.77	0.20	0.31
YELL+	12.09	2.35	12.22	15.97	19.02	18.19	13.17	3.11	0.78	0.17	0.28
ZWEN									1.00	0.37	0.58
ZWEN*	12.62	4.00	24.17	-8.25	15.66	8.08	18.62	-36.71	0.76	0.40	0.49
ZWEN&	12.62	4.00	27.95	15.62	15.15	15.29	23.63	16.84	0.72	0.31	0.49
ZWEN /	12.67	4.02	29.58	11.13	6.86	8.08	21.98	30.43	0.70	0.33	0.54
ZWEN%	0	0	17.04	7.31	17.30	14.28	16.14	53.96	0.83	0.34	0.48
ZWEN+	12.09	3.90	24.26	14.20	25.50	22.05	23.54	34.08	0.76	0.32	0.43

Acknowledgments

We wish to thank Per Jarlemark and Jan Johansson of the Onsala Space Observatory for supplying the Onsala WVR data. The work described in his paper was carried out in part by the Jet Propulsion Laboratory, California Institute of Technology, under contract with the National Aeronautics and Space Administration.

References

Bar-Sever, Y.E. and P.M. Kroger, Strategies for GPS-Based Estimates of Troposphere Delay, *Proceedings of the 9th International Technical Meeting of The Institute of Navigation*, Kansas City, MO, September 17-20, 1996.

Bar-Sever, Y.E., Strategies for Near Real Time Estimates of Precipitable Water Vapor, *Proceedings of the IGS workshop*, Silver Springs, MD, May, 1996

Bevis, M., S. Chiswell, S. Businger, T.A. Herring and Y. Bock, Estimating Wet Delays Using Numerical Weather Analyses and Predict ions, *Radio Science*, Vol. 31, pp 477-487, May-June 1996.

Bevis, M., S. Businger, S. Chiswell, T.A. Herring, R.A. Anthes, C. Rocken and R.H. Ware, GPS Meteorology: Mapping Zenith Wet Delays onto Precipitable Water, *Journal of Applied Meteorology*, Vol. 33, No. 3, March 1994.

Businger, S., S.R. Chiswell, M. Bevis, J. Duan, A. Anthes, C. Rocken, R.H. Ware, M. Exner, T. VanHove and F.S. Solheim, The Promise of GPS in Atmospheric Monitoring, *Bull. Am. Met. SW.*, Vol. 77, No. 1, January, 1996.

Chen, G. and T.H. Herring, Effects of Atmospheric Azimuthal Asymmetry on the Analysis of Space Geodetic Data, *J. Geophys. Res.*, in press, 1997.

Chiswell, S.R. and S. Businger, Improved Severe Weather Forecasts Using GPS, IUGG XXI General Assembly, Boulder, CO, July, 1995.

Davis, J. L., T.A. Herring, 1.1. Shapiro, A.E.E. Rogers, and G. Elgered, Geodesy by Radio Interferometry: Effects of Atmospheric Modeling Errors on Estimates of Baseline Length, *Radio Science*, 20, pp 1593-1607, 1985.

Davis, J. L., G. Elgered, A.E. Niell and C.E. Kuehn, Ground-Based Measurements of the Gradients in the "Wet" Radio Refractivity of Air, *Radio Science*, Vol. *28, No. 6* pp. 1003-1018, November-December, 1993.

Duan, J., M. Bevis, P. Fang, Y. Bock, S. Chiswell, S. Businger, C. Rocken, F. Solheim, T. Van Hove, R. Ware, S. McClusky, T. Herring and R. King, GPS Meteorology: Direct Estimation of the Absolute Value of Precipitable Water, *J. App. Meteor.*, Vol. 35, No. 6, June 1996.

Elgered, G., J.M. Johansson and B. Lindgren, Using the Swedish GPS Network to Monitor the Atmospheric Water Vapor Content, IUGG XXI General Assembly, Boulder, CO, July 1995.

Gardner, C. S., Correction of Laser Tracking Data for The Effects of Horizontal Refractivity Gradients, *Appl. Opt., 16,* pp. 2427-2432, 1977.

Heflin, M., M. Watkins, D. Dauger, GPS Time Series: Noise Characteristics based on 55405 Station-Days (abstract), 10S *Trans. AGU, S72,* 1996.

Heflin, M., D. Jefferson, Y. Vigue, F. Webb, J. Zumberge, D. Argus and G. Blewitt, Vertical Rates Determined With The Global Positioning System (abstract), *EOS Trans. AGU*, 75(16), Spring Meeting Suppl., 104, 1994.

Herring, T. A., Modeling Atmospheric Delays in the Analysis of Space Geodetic data, *Refraction of Transatmospheric Signals in Geodesy,* eds. J.C. Munck and T.A. Spoelstra, Netherlands Geodetic Commission Publications in Geodesy, 36, pp. 157-164, 1992.

IGS report 4112, http://igscb.jpl.nasa.gov/mail, 1997.

IGS 1995 Annual Report, Jet Propulsion Laboratory, Pasadena, CA, September, 1996.

Lanyi, G., tropospheric Delay Effects in Radio Interferometry, TDA Progress Report, 42-78, Vol. April-June 1984, Jet Propulsion laboratory, Pasadena, California, August 15, 1984.

MacMillan, D. S., Atmospheric Gradients From Very Long Baseline Interferometry Observations, *Geophys. Res. Left.,* Vol. 22, No. 9, pp. 1041-1044, Mat, 1995.

MacMillan, D.S. and C. Ma, Evaluation of Very Long Baseline Interferometry Atmospheric Modeling Improvements, *J. Geophys. Res.*, 99 (B 1), p. 637-651, 1994.

Niell, A. H., Global Mapping Functions for the Atmospheric Delay at Radio Wavelengths, *J. Geophys. Res.*, Vol. 101, pp. 3227-3246, 1996.

Rocken, C., T. VanHove, R. Chadwick, S. Gutman, D. Wolfe and E. Westwater, Long Term Results From a Network of Global Positioning Receivers for Water Vapor Meteorology, IUGG XXI General Assembly, Boulder, CO, July, 1995.

Runge, T. F., P.M. Kroger, Y.E. Bar-Sever and M. Bevis, Accuracy Evaluation of Ground-based GPS Estimates of Precipitable Water Vapor (abstract), *EOS Transactions,* American Geophysical Union, 1995 Fall Meeting, Vol. 76,1:146.

Saastamoinnen, J., At mospheric Correct ion for the Troposphere and Stratosphere in Radio Ranging of Satellites, *The Use of Artificial Satellites for Geodesy, Geophys. Mongogr.*, Ser. 15, Amer. Geophys. Union, pp 247-251, 1972.

Wolfe, D.E. and S.1. Gutman, Comparing Changes in GPS Perceptible water Vapor to Vertical Profiles of Precipitable Water Vapor (abstract), *EOS Trans. AGU*, Supplement 174, 1994.

Ware, R., C. Alber, C. Rocken, F. Solheim, Sensing Integrated Water Vapor Along GPS Ray Paths, *Geophys. Res. Lett.* 24, pp 417-420, 1997.

Zumberge, J .F., M.B. Heflin, D.C. Jefferson., M.M. Watkins and F.H. Webb, Precise Point Positioning for the Efficient and Robust Analysis of GPS Data from Large Networks, *J. Geophys. Res.*, Vol. 102, No. B3, pp 5005-5017, March, 1997.

Zumberge, J .F., M.B. Heflin, D.C. Jefferson., M.M. Watkins and F.H. Webb, IGS Analysis Center 1994 Annual Report, JPL Publication 95-18, Jet Propulsion Laboratory, Pasadena, CA, September 1, 1995.

Figure Captions

Figure 1. Improvement in 3D position repeatability due to the nominal inhomogeneous strategy relative to the nominal homogeneous strategy, plotted as a function of the percentage of low elevation angle measurements. 149 IGS sites included. The mean improvement over all sites was 1.6%.

Figure 2. Median formal errors of the cst imated gradients with the nominal inhomogeneous strategy as a function of the mean dai I y percent age of measurements bet wccn 7° and 150. nominal inhomogeneous strategy as a function of the mean daily percentage of measurements between 7° elevation angle cutoff was used. For each site the median was taken over all output epochs (every 5 minutes) during October - December, 1996. The formal errors for the estimates of the position vector show a similar pattern. Three sites with very little data overall, and hence high formal errors, were excluded.

Figure 3. Tuning the estimation strategy for site AOA1 in southern California, Performance is measured as improved repeatability in the radial coordinate when comparing to the nominal homogeneous strategy.

Figure 4. Formal errors in the magnitudes and azimuths of the GPS - and WVR-based gradients. a. Formal errors in the magnitudes of the GPS-based gradients as percentage of the magnitudes. b. same as in a but for the WVR. c. Formal errors in the azimuths of the GPS-based gradients. d. Same as in c but for the WVR.

Figure 5. The observed hydrostatic gradients derived as the vector biases between the GPS-based gradients and the WVR-based gradient for each 12-hour segment. Left: azimuth, right: magnitude.

Figure 6. Magnitude of the (debiased) GPS-based gradient vector plotted against the magnitude of the WVR-based estimates of the gradient vector. The slope of line that fits the data in a weighted least square sense is shown in the inset box together with its standard deviation.

Figure 7. Differences in the azimuths between the GPS- and the WVR-based estimates of the gradient vectors as a function of the WVR-based magnitude of the vector.

Figure 8. GPS- and WVR-based estimates of G_N (top) and G_E (bottom) for 6 12-hour segments during October 1995. Note, the bias between the GPS and the WVR estimates for each segment was removed. Only 6 segments are shown for clarity. Other segments are similar. The absence of every other 12-hour segment is a result of the requirement for having a WVR data point at least every 15 minutes. Most 12-hour segments centered on noon did not fulfill this requirement for unknown reasons. The midnight-centered segments include the day's boundary and can display, therefore, some discontinuity in the estimates. Such discontinuities can be observed with G_N in the 5th and 6th segments.

Figure 9. Az-el distribution of observations by the ONSA GPS receiver during October 14, 1995. North is 0°. East is 90°.

Figure 10. Magnitude and azimuth of the WVR-based gradients. North is 0°. East is 90°.

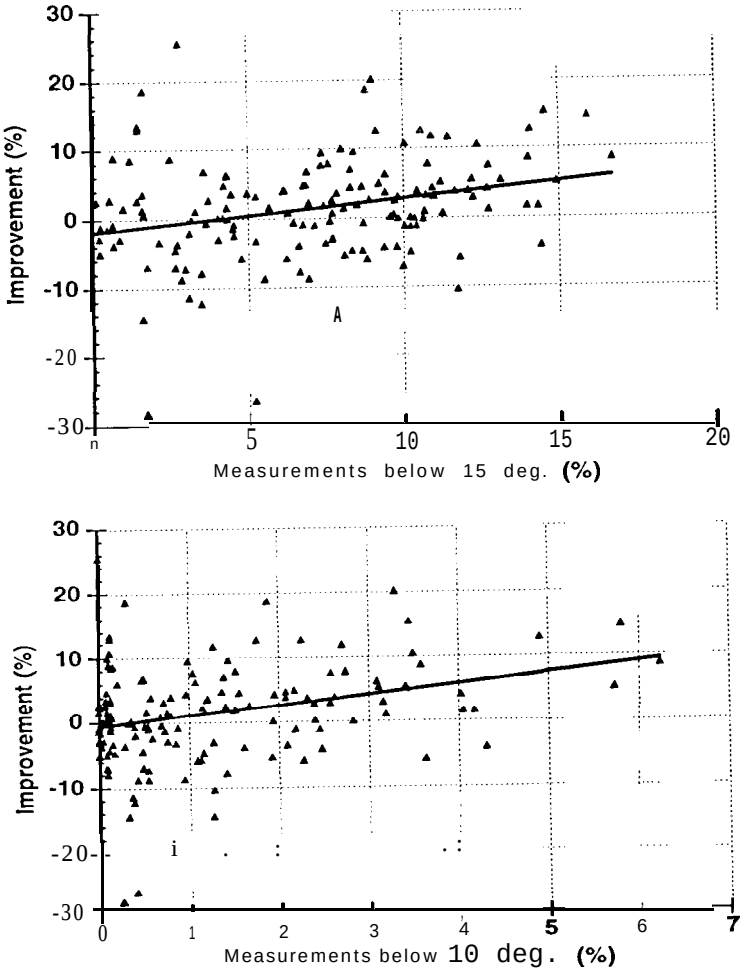

Figure 1.

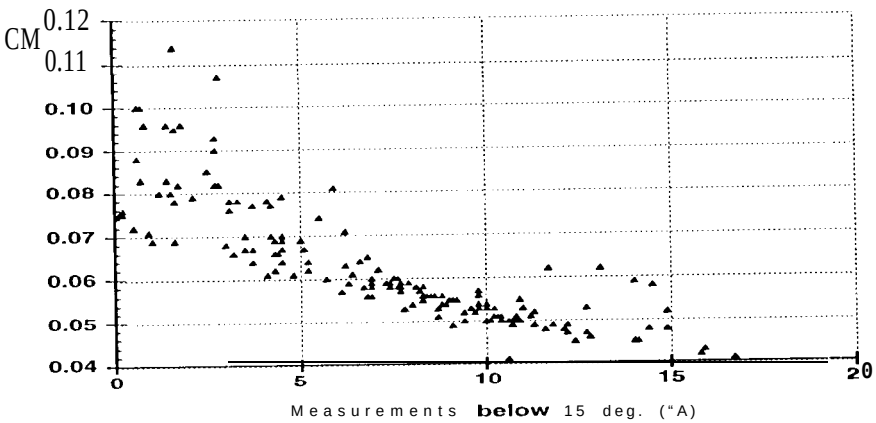

Figure 2.

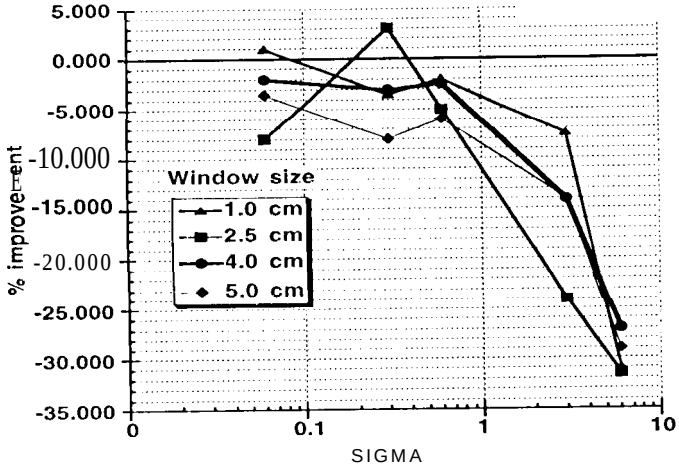
5.000
0.000
-5.000
-10.000
-15.000
-20.000
-25.000
-30.000
-35.000
% improvement
Window size
1.0 cm
2.5 cm
4.0 cm
5.0 cm
0
0.1
1
10
SIGMA

Figure 3.

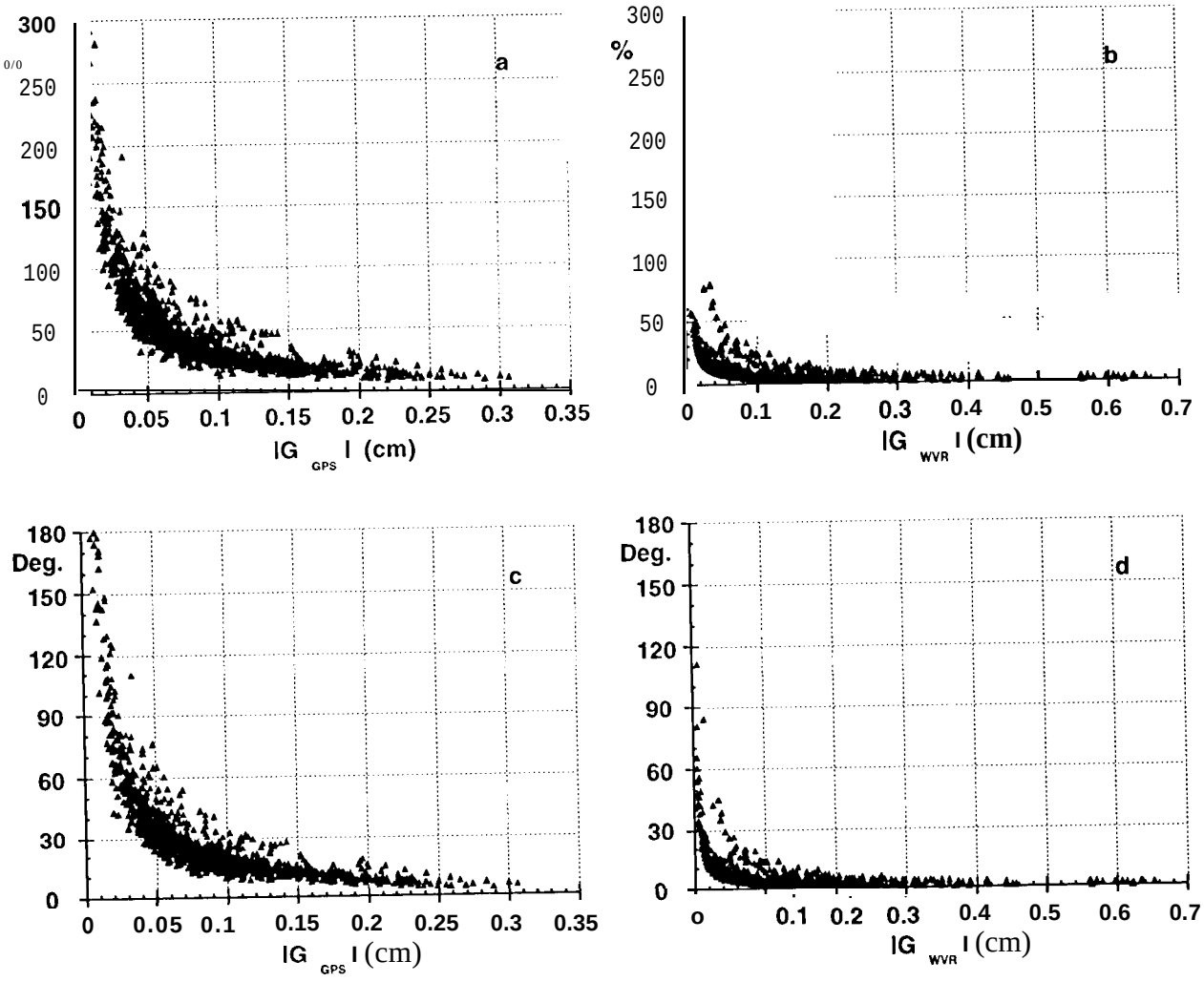
300
0/0
250
200
150
100
50
0
0 0.05 0.1 0.15 0.2 0.25 0.3 0.35
IG GPS I (cm)
a
300
%
250
200
150
100
50
0
0 0.1 0.2 0.3 0.4 0.5 0.6 0.7
IG WVR I (cm)
b
180
Deg.
150
120
90
60
30
0
0 0.05 0.1 0.15 0.2 0.25 0.3 0.35
IG GPS I (cm)
c
180
Deg.
150
120
90
60
30
0
o 0.1 0.2 0.3 0.4 0.5 0.6 0.7
IG WVR I (cm)
d

Figure 4.

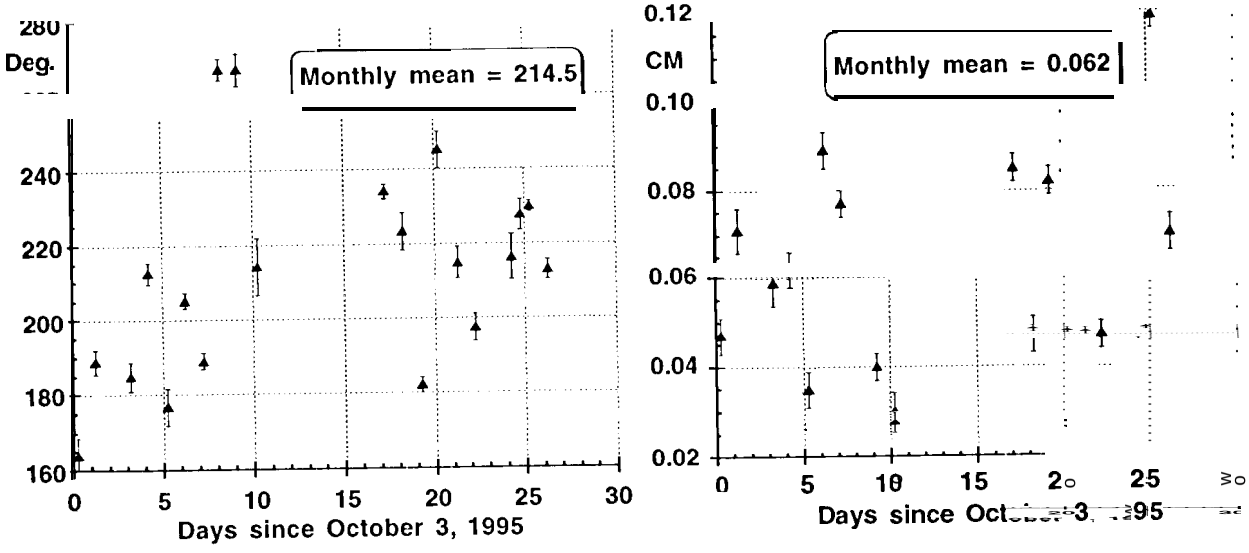

Figure 5.

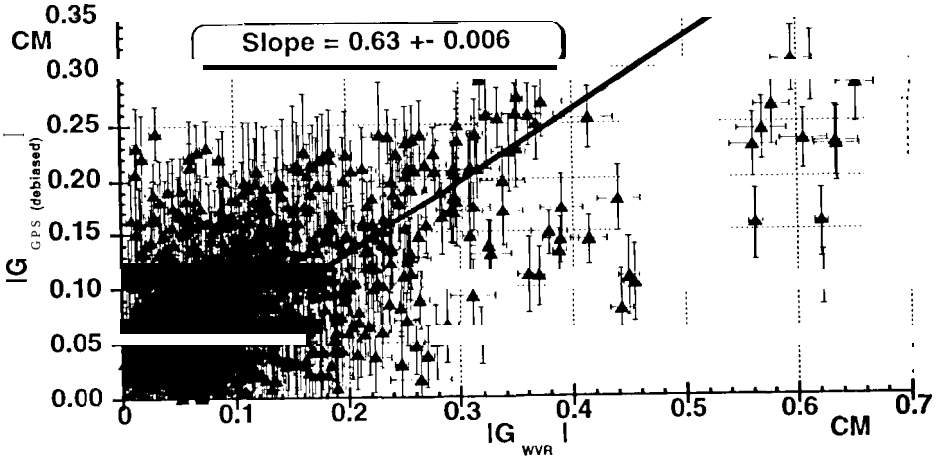

Figure 6.

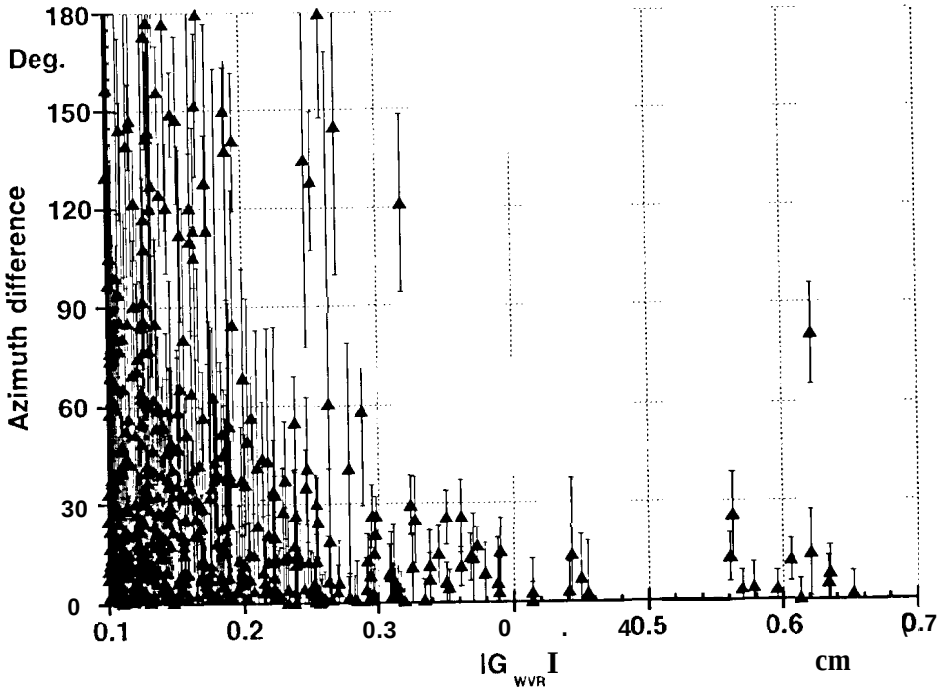
180
Deg.
150
120
90
60
30
0
Azimuth difference
0.1
0.2
0.3
0.5
0.6
0.7
|G WVR I
cm

Figure 7.

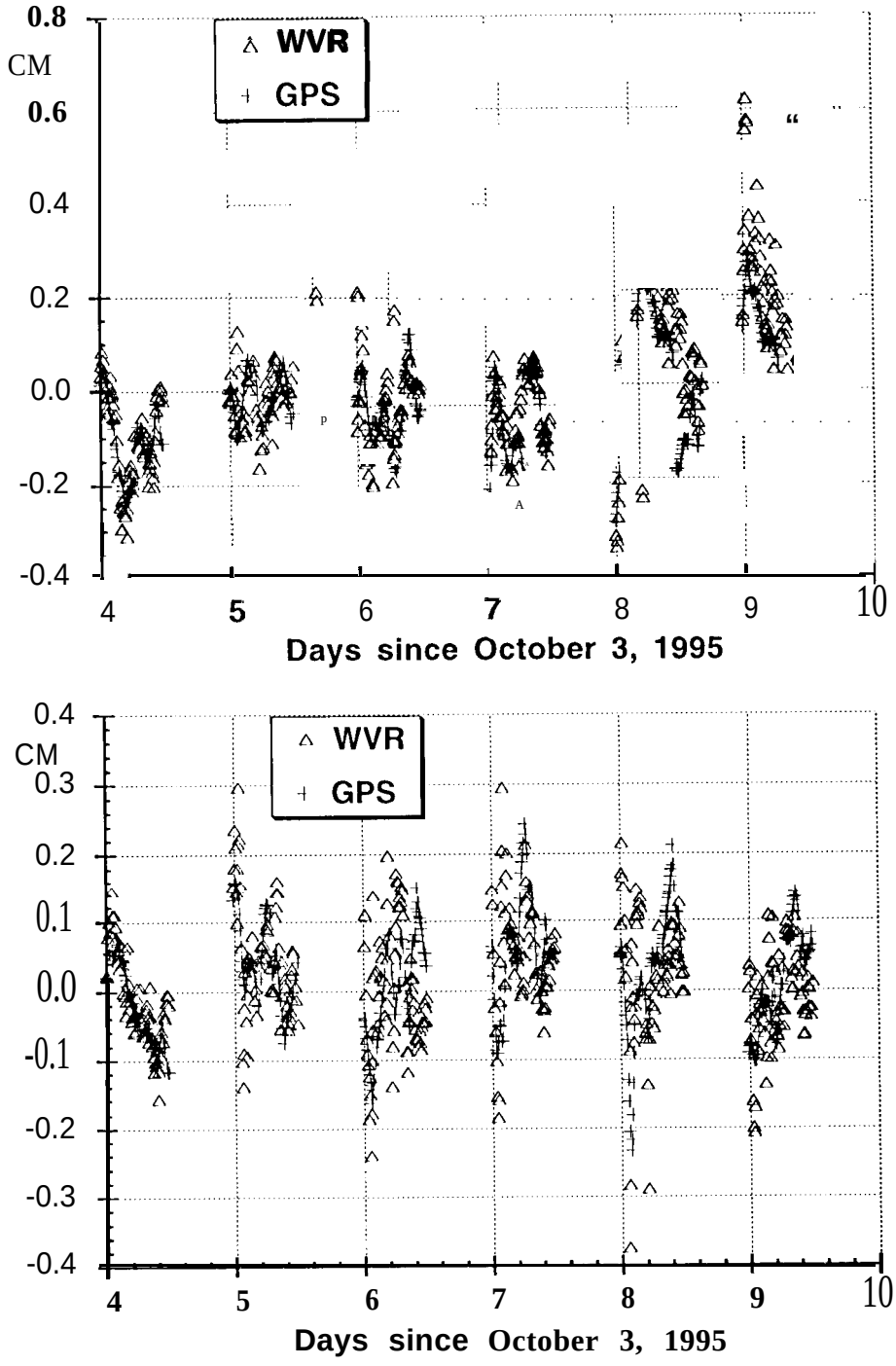
0.8
CM
0.6
0.4
0.2
0.0
-0.2
-0.4
WVR
GPS
4
5
6
7
8
9
10
Days since October 3, 1995
0.4
CM
0.3
0.2
0.1
0.0
-0.1
-0.2
-0.3
-0.4
WVR
GPS
4
5
6
7
8
9
10
Days since October 3, 1995

Figure 8.

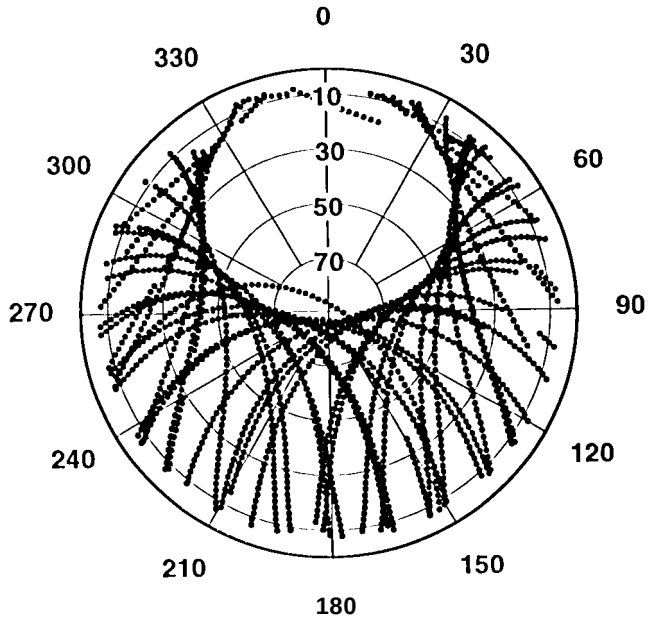

Figure 9.

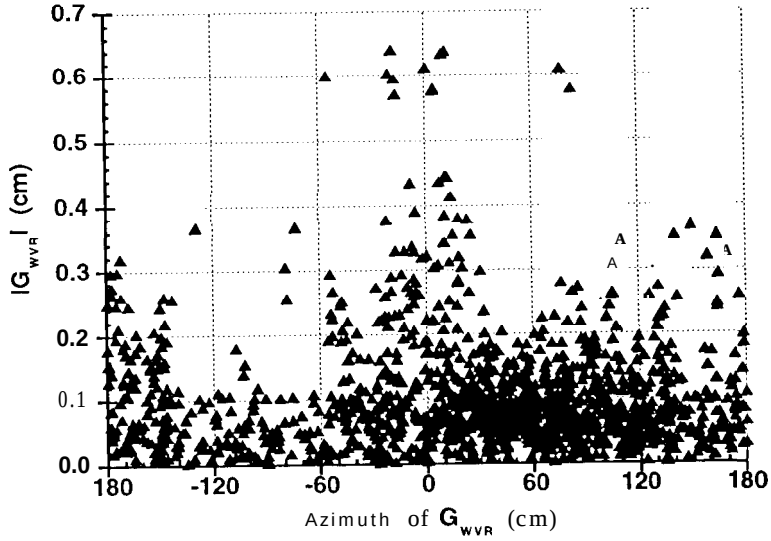

Figure 10.

Table 1. Differences between estimation strategies.

Estimation strategy	Elevation angle cutoff (°)	Sigma for D_{wz} (mm/√hour)	Sigma for G_N and G_E (mm/√hour)	Post-fit window (cm)
Current JPL	15	10.2	Not modeled	5
Nominal homogeneous	7	3	Not modeled	5
Nominal inhomogeneous	7	3	0.6	5
Constant gradient	7	3	0.0	5
Tuned inhomogeneous	7	3	0.3	2.5
Tuned 15°	15	3	0.3	2.5

Table 2. Mean improvement in position repeatability due to each strategy.

Strategy	Radial	Horizontal	3D
Nominal homogeneous	9.3%	-3.7%	5.4%
Nominal inhomogeneous	13.4%	2.6%	10.2%
Constant gradient	12.3%	2.8%	9.770
Tuned inhomogeneous	19.5%	15.2%	18.570
Tuned 15°	11.0%	11.670	11.7%

improvement is measured relative to the current JPL strategy. Based on the 37 sites with more than 2% of all measurements between 10° and 7°.

Table 3. Average absolute coordinate biases between pairs of estimation strategies for the 37 sites with more t ban 2% of al 1 measurements bet wccn 1 0° and 7°. In cent imeters.

Strategies	Radial	Latitude	Longitude
Current JPL & nominal homogeneous	1.22	0.08	**0.08**
Current JPL & t uned i nhomogeneous	0.99	0.12	0.10
Nominal homogeneous & tuned inhomogeneous	0.30	0.19	0.11
Current JPL & tuned 15°	0.30	0,14	0.13

Table 4. Mean and scatter around the mean (sigma) of WVR minus GPS estimates of **ZWD,** in centimeters, for GOL3 and ONSA. The GOL3 comparison includes 3797 data points. The ONSA comparison includes 935 data points.

	GOL3		ONSA	
Strategy	Mean (WVR-GPS)	Sigma (WVR-GPS)	Mean (WVR-GPS)	Sigma (WVR-GPS)
Current JPL	0.382	0.545	-0.396	0.711
Nominal homogeneous	0.122	0.535	-0.041	0.550
Tuned inhomogeneous	0.095	0.488	-0.041	0.507

Table 5. Formal errors in the GPS- and WVR-based estimates of the troposphere gradients. In centimeters.

	GPS		WVR	
Gradient component	Mean	Sigma	Mean	Sigma
G_N	0.033	0.008	0.007	0.004
G_E	0.030	0.009	0.007	0.004

Table 6. Statistics of the difference between GPS- and WVR-estimates of the troposphere gradients.

Subset	Mean relative magnitude of difference	Mean azimuth difference	Linear correlation in magnitude	Slope of linear fit for magnitude
All points (1374)	63%	29°	0.56	0.63
$\lvert G_{WVR}\rvert > 0.1$ cm (490)	58%	19°	0.50	0.56
$\lvert G_{WVR}\rvert > 0.2$ cm (1 35)	55%	10°	0.38	0.49
$\lvert G_{WVR}\rvert > 0.3$ cm (46)	60%	8°	0.21	0.43
$\lvert G_{WVR}\rvert < 0.3$ cm (1 328)	66%	33°	0.49	0.75
$\lvert G_{WVR}\rvert < 0.2$ cm (1237)	75%	38°	0.37	0.84
$\lvert G_{WVR}\rvert < 0.1$ cm (878)	96%	46°	0.22	1.1

Four statistical parameters are computed for 7 subsets of the complete data set of 1374 points. The statistical parameters are:

1. Mean relative magnitude of difference, i.e., the weighted mean of 100 $\lvert G_{WVR} - G_{GPS}\rvert / \lvert G_{WVR}\rvert$.
2. Mean azimuth difference, i.e., the weighted mean of $\lvert \angle G_{GPS} - \angle G_{WVR}\rvert$.
3. The weighted linear correlation (also known as Pearson's r) between $\lvert G_{GPS}\rvert$ and $\lvert G_{WVR}\rvert$.
4. The slope of the line with zero intercept that best fit the set of pairs $(\lvert G_{GPS}\rvert, \lvert G_{WVR}\rvert)$ in a weighted least squares sense.